Nonstandard-Higgs-scalar- and pseudoscalar-boson production in ep and e^+e^- colliders

R. Bates and John N. Ng
Theory Group, TRIUMF, 4004 Wesbrook Mall, Vancouver, British Columbia, Canada V6T 2A3
(Received 7 August 1985)

Nonstandard Higgs bosons in the mass range 40—150 GeV/c^2 are studied for two-Higgs-doublet extensions of the standard electroweak model. Upper bounds on production rates are compared for ep and e^+e^- colliders. Under favorable conditions our calculations indicate that about 100 events per year production rates at the DESY ep collider HERA for nonstandard Higgs bosons are obtainable. Electron-positron annihilations give smaller rates but cleaner signals.

I. INTRODUCTION

In this paper we study the production in electron-proton and e^+e^- colliders of scalar bosons ($J^{PC}=0^{++}$) which we denote by S^0, and pseudoscalar bosons ($J^{PC}=0^{--}$) denoted by P^0 which are contained in extensions of the standard Glashow-Weinberg-Salam electroweak theories. These bosons, including that from the standard model, are collectively denoted by H^0. The ep semi-inclusive reactions studied are

$$e+p\rightarrow e+S^0+X \tag{1.1a}$$

$$\rightarrow e+P^0+X\ , \tag{1.1b}$$

where X denotes any hadronic states. We shall assume the quark-parton model for the collision in Eq. (1.1). The electron-quark scattering subprocesses are

$$e(l)+Q(q)\rightarrow e(l')+S^0(h)+Q(q') \tag{1.2a}$$

$$\rightarrow e(l')+P^0(h)+Q(q')\ , \tag{1.2b}$$

where Q denotes either the u- or d-type quark in the proton. In Eq. (1.2), the four-momenta of the various particles are given in their respective parentheses.

It is well known that in the standard model with one Higgs doublet and three quark-lepton families, the production rate for the Higgs boson is distressingly small[1] for an ep collider such as DESY HERA. This can be understood by examining the production mechanism for reaction (1.2a). In ep collisions, Higgs-boson production proceeds via the t-channel processes depicted in Figs. 1(a) and 1(b). The process of Fig. 1(a) is suppressed by the two Z^0 propagators, although this is partly compensated by the large H^0ZZ coupling. On the other hand, the process in Fig. 1(b) has no such suppression but is enhanced by the double-photon-exchange poles. However, the $H^0\gamma\gamma$ vertex is of higher order in the standard model, thereby rendering this amplitude small. In most cases the amplitude of Fig. 1(a) is larger in size than that of Fig. 1(b). Enhancement of the effective $H^0\gamma\gamma$ coupling can be achieved by introducing more quark-lepton families, but it is not sufficient to push the production rate to observable levels unless the number of extra families is incredibly large ($\gtrsim 35$). For details see Sec. II.

More optimistic situations can occur in extensions of the standard model. One of the simplest is to add a second Higgs doublet to the standard model. After symmetry breaking one is left with two charged Higgs bosons and three neutral spin-0 particles, of which two are scalars and one is a pseudoscalar. In addition to being of interest in its own right, the two-Higgs-doublet model is required in supersymmetry extensions of the standard model.[2] In general, both the $S^0\gamma\gamma$ and $P^0\gamma\gamma$ vertices can be enhanced substantially in these models. This makes the photon exchange amplitude dominate over the Z^0-exchange one. In this paper we shall study quantitatively how much enhancement is allowed by current knowledge and give estimates of the production rates for such particles at HERA using a luminosity of 6×10^{31} cm^{-2}s^{-1}.

It is a common feature of such models that the tree-level H^0ZZ coupling is changed at most by a mixing angle and possible enhancement can come from the $S^0\gamma\gamma$ and $P^0\gamma\gamma$ vertices. We shall concentrate on the production due mainly to Fig. 1(b). This allows us to use the

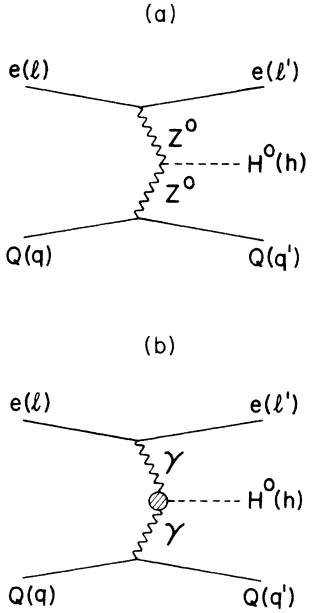

FIG. 1. Feynman diagrams for Higgs-boson production in the reaction $eq\rightarrow eqH^0$. (a) t-channel Z-boson exchange; (b) t-channel photon exchange.

equivalent-photon approximation[3] (EPA) to estimate the production rate. We first calculate the cross section for subprocesses in Eqs. (1.2a) and (1.2b) using EPA, and then convolute it with the well-known parton distribution functions of the quark-parton model. The EPA has been demonstrated to be good to within 10% in resonance production in $e\bar{e}$ collisions, and it is expected to be of the same accuracy in ep collisions. As a check we also calculated the production rate using the Monte Carlo method, and the results agree to within the accuracy of the Monte Carlo method.

In the same view we also consider the production of S^0 and P^0 in e^+e^-. The purpose is to compare the relative strengths of the above two types of colliders for scalar and pseudoscalar production. The reactions we consider here are the ones similar to Eq. (1.1), namely,

$$e\bar{e}\rightarrow e\bar{e}S^0 , \tag{1.3a}$$

$$e\bar{e}\rightarrow e\bar{e}P^0 . \tag{1.3b}$$

The case where H^0 is the standard-model Higgs boson was studied in Ref. 4. However, the authors have a constructive interference between the s- and t-channel amplitudes whereas we found a destructive one.[5] This agrees with a recent calculation of Ref. 6. Detailed predictions with the mass of the Higgs boson ranging from 40 to 150 GeV/c^2 can be obtained there. We note that the cross sections are of the order of 10^{-3} pb and hence would be very difficult for the CERN electron-positron collider LEP or the Stanford Linear Collider (SLC) to detect.

Since we are interested in cases where the $S^0\gamma\gamma$ and/or $P^0\gamma\gamma$ vertices are enhanced we can concentrate on the two-photon production mechanism. This is the same as Fig. 1(b) with quark lines being replaced by e^+ lines. The calculation is the same as for the ep case but one does not need to convolute over parton distributions.

In Sec. II we give the results for standard-model one-Higgs-boson production. This serves as a benchmark for the subsequent discussions of nonstandard spin-0 particle production. Our results overlap with that given in Ref. 1 and we agree with their calculation. However, no details were given there. Section III gives a brief discussion of the two-Higgs-doublet model with the relevant vertices displayed. Enhancement effects are discussed. The effects of charged scalar loops are also shown to be small. Finally Sec. IV gives a comparison between ep and e^+e^- colliders for S^0 and P^0 productions.

II. STANDARD-MODEL HIGGS-BOSON PRODUCTION

The Higgs boson can be produced in ep collisions via Z^0-Z^0 [see Fig. 1(a)] and photon-photon [see Fig. 1(b)] collisions. The two-photon process is generally dominated by the two-Z^0 mechanism. At HERA energies for Higgs-boson mass $M_H < M_W$, the two-Z^0 fusion cross section is about an order to magnitude larger. However, it is still of interest to outline the calculation of the two-photon resonance production of the Higgs boson as this will give us a reference to compare with later calculations.

The photon-exchange production cross section can be obtained in terms of the 2γ decay width of the Higgs boson. There are three classes of diagrams contributing to this width: namely, fermion loops, gauge-boson loops, and scalar loops. Representative diagrams are displayed in Figs. 2(a)–2(c). A complete set of diagrams and Feynman rules are listed in Ref. 7. It turns out that the gauge-boson loops give the dominant contribution while the t-quark loop (with $m_t = 40$ GeV/c^2) gives the only other significant contribution. The scalar loops and loops of all other known fermions give a negligible contribution in the standard model. If we write the gauge-invariant amplitude M for $H^0\rightarrow\gamma(k_1)+\gamma(k_2)$ as

$$M = A\, e_1^{\mu} e_2^{\nu}(g_{\mu\nu} - k_{1\nu}k_{2\mu}/k_1\cdot k_2) , \tag{2.1}$$

where e_1 and e_2 are polarization vectors of the two photons, then the structure function A is given by[1,6]

$$A = \frac{i\,e^2 g M_H^{\,2}}{8\pi^2 M_W}(A_W + A_F + A_S) , \tag{2.2a}$$

where

$$A_W = \frac{3M_W^{\,2}}{M_H^{\,2}} + \frac{2M_W^{\,2}}{M_H^{\,2}}\left[2 - \frac{3M_W^{\,2}}{M_H^{\,2}}\right] I\left[\frac{M_W^{\,2}}{M_H^{\,2}}\right] , \tag{2.2b}$$

$$A_F = -\sum_f \frac{Q_f^{\,2} m_f^{\,2}}{M_H^{\,2}}\left[2 - \left[\frac{4m_f^{\,2}}{M_H^{\,2}} - 1\right] I\left[\frac{m_f^{\,2}}{M_H^{\,2}}\right]\right] , \tag{2.2c}$$

$$A_S = \frac{1}{2} - \frac{M_W^{\,2}}{M_H^{\,2}} I\left[\frac{M_W^{\,2}}{M_H^{\,2}}\right] , \tag{2.2d}$$

and

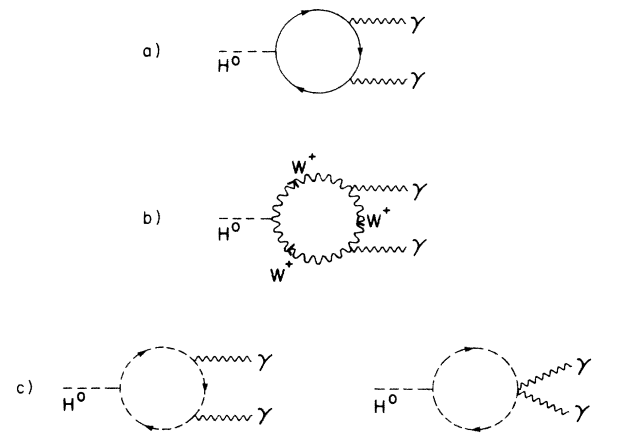

FIG. 2. Some representative examples of the Feynman diagrams which contribute to the 2γ decay width of the Higgs boson (a) fermion loop, (b) gauge-boson loop, and (c) scalar loop. The ghost loops and four-point interactions are not shown for (b).

$$I(\lambda)=\begin{cases}2\left[\arcsin\left[\dfrac{1}{2\sqrt{\lambda}}\right]\right]^2, & \lambda>\frac{1}{4}, \\ \dfrac{\pi^2}{2}-2\ln^2\left[\dfrac{1+(1-4\lambda)^{1/2}}{2\sqrt{\lambda}}\right] \\ \quad +2i\pi\ln\left[\dfrac{1+(1-4\lambda)^{1/2}}{2\sqrt{\lambda}}\right], & \lambda<\frac{1}{4}. \end{cases} \quad (2.2e)$$

The quantities A_W, A_F, A_S correspond to contributions from gauge-boson loops (including ghosts and would-be Goldstone bosons), fermion loops and scalar loops, respectively. The sum in Eq. (2.2c) is taken over all charged-fermion species. The separation above is for convenience since the standard model has no physical charged scalars, so the scalar loop of Fig. 2(c) consists of only would-be Goldstone bosons.

Next we calculate the cross section of the subprocess Eq. (1.2a) with the EPA. Using the photon spectrum given in Ref. 8 we obtain

$$\hat{\sigma}_q(\hat{s})=\frac{\alpha^2 Q_q^2|A|^2}{4\pi M_H^4}\ln\left[\frac{\hat{s}}{m_e^2}\right]\left[\ln\left[\frac{M_H^2}{m_q^2}\right][\rho^2+2\rho-3-(2+2\rho+\tfrac{1}{2}\rho^2)\ln\rho]+\frac{\rho^2}{4}\ln^2\rho+(2\rho^2+4\rho-6)\ln(1-\rho)\right.$$
$$-(\tfrac{5}{2}\rho^2+4\rho-5)\ln\rho+(\tfrac{25}{4}-6\rho-\tfrac{1}{4}\rho^2)$$
$$\left.+(\rho^2+4\rho+4)[-Li(1)+Li(\rho)+\tfrac{1}{2}\ln^2 p]\right], \quad (2.3)$$

where $\rho\equiv M_H^2/\hat{s}$ and $\hat{s}\equiv(l+q)^2$. The quark charges are given by Q_q. Also

$$\mathrm{Li}(x)\equiv-\int_0^x dt\,\ln(1-t)/t\ .$$

The quark-parton model is then used to estimate the cross section for the physical process of Eq. (1.1a) by convoluting over the quark distribution functions $f_q(x)$. Explicitly

$$\sigma=\int_{M_H^2/s}^1 dx\sum_q f_q(x)\sigma_q(xs)\ . \quad (2.4)$$

This last integration is done numerically.

In Fig. 3 we give the cross section as a function of $\sqrt{s}$ for two values of $M_H=40$ and 150 GeV/c^2. In accordance with previous calculations[1] this cross section is distressingly small, typically on the order of 10^{-40} cm^2. The lower curve in Fig. 4 depicts the cross section as a function of the Higgs-boson mass for $\sqrt{s}=320$ GeV, appropriate for HERA. We also indicate the cross section due to the two-Z^0-boson fusion mechanism alone. Similar curves for $\sqrt{s}=1$ TeV are shown in Fig. 5. Although obscured in Fig. 4 by the effects of phase space, there is a rise in the photon-exchange cross section for large M_H, which is very apparent in Fig. 5. This rise is due to the behavior of the function $I(\lambda)$ in Eq. (2.2e) near $\lambda=\frac{1}{4}$. The Re$[I(\lambda)]$ peaks at $\lambda=\frac{1}{4}$, while Im$[I(\lambda)]=0$ for $\lambda>\frac{1}{4}$ and peaks between $\lambda=0$ and $\lambda=\frac{1}{4}$. The dominant

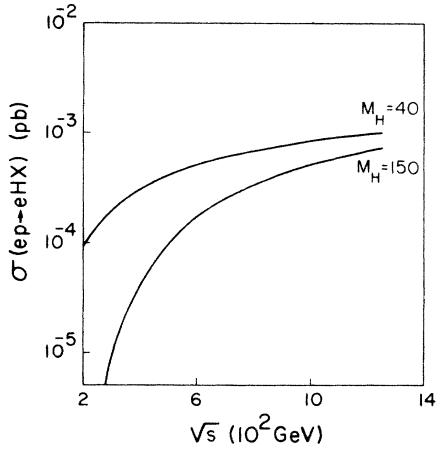

FIG. 3. Photon-exchange production cross sections of the standard model for $ep\to eH^0X$ as a function of $\sqrt{s}$ with $M_H=40$, 150 GeV/c^2.

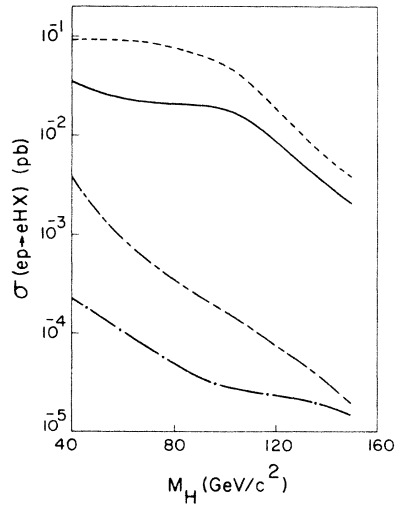

FIG. 4. Production cross sections for $ep\to eH^0X$ as a function of M_H for $\sqrt{s}=320$ GeV. The dash-dot (dashed) curve is for standard-model photon (Z-boson) exchange. The solid (broken) curve is for two-Higgs-doublet model photon-exchange scalar (pseudoscalar) production with $\tan\alpha=40$.

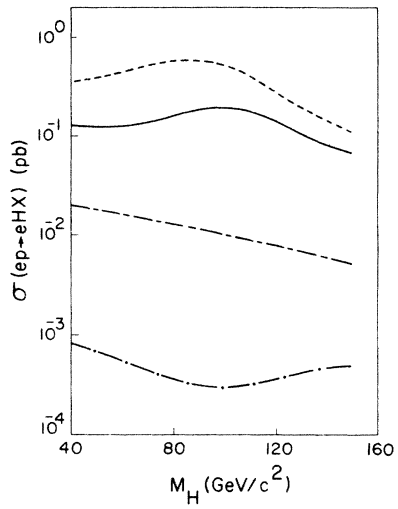

FIG. 5. Production cross sections for $ep \to eH^0X$ as a function of M_H for $\sqrt{s}=1$ TeV. The dash-dot (dashed) curve is for standard model photon (Z-boson) exchange. The solid (broken) curve is for two Higgs doublet model photon-exchange scalar (pseudoscalar) production with $\tan\alpha=40$.

contribution to the standard-model photon-exchange cross section is the gauge-boson loop of Eq. (2.2b), which contains $I(M_W{}^2/M_H{}^2)$. Hence as M_H increases, the cross section will rise with $\mathrm{Re}[I(M_W{}^2/M_H{}^2)]$ and peak once M_H gets above twice the W-boson mass as determined by Eq. (2.2b).

We now note several important points here about two-photon resonance production of the standard Higgs boson. The first one is that the gauge-boson loop gives the largest amplitude for a wide range of M_H values, and is about a factor of 5 larger than the next contribution due to the t-quark loop. The other fermion loops and the scalar loop are unimportant. Second, the gauge-boson loop and the fermion-loop amplitudes have opposite signs. Third, once the ratio m_f/M_H is greater than $\frac{1}{2}$, the amplitude A_F in Eq. (2.2c) is fairly insensitive to the internal mass m_f. The combined effect of these points is that introducing an additional heavy fermion into the standard model will decrease the production rate. To enhance the rate in this way one has to introduce many families. Five heavy charged fermions are needed in A_F to cancel A_W, and at least 30 more are necessary to bring the cross section up to 10^{-38} cm^2, which would be observable for a machine of HERA's luminosity.

Our prognostication for the standard Higgs-boson production in ep collisions is that it is not competitive with $e\bar{e}$ or pp collisions. At $\sqrt{s}=320$ GeV the two-Z^0 mechanism dominates and the cross section is at least one order of magnitude too small for observation even for light Higgs bosons. For $\sqrt{s}=1$ TeV the two-Z^0 mechanism becomes just large enough if the same luminosity can be maintained. The production rate for the two-photon process is too low in the standard model, and becomes important only if there exists a large number of heavy charged fermions. We note that the standard Higgs-boson production cross section for $e\bar{e}$ collisions via the same mechanism is given by Eq. (2.3) with $\hat{s}$ replaced by s, the center-of-mass energy of the $e\bar{e}$ system.

III. TWO-HIGGS-DOUBLET MODEL

In models with two Higgs doublets given by

$$\Phi_1=\begin{bmatrix}\phi_1^+\\ \phi_1^0\end{bmatrix},\quad \Phi_2=\begin{bmatrix}\phi_2^+\\ \phi_2^0\end{bmatrix} \tag{3.1}$$

the vacuum is characterized by two vacuum expectation values (VEV's)

$$\langle\Phi_1\rangle=\begin{bmatrix}0\\ \frac{a}{\sqrt{2}}\end{bmatrix},\quad \langle\Phi_2\rangle=\begin{bmatrix}0\\ \frac{b}{\sqrt{2}}\end{bmatrix}. \tag{3.2}$$

We define the rotated fields,

$$\begin{aligned}\Phi_1'&=\Phi_1\cos\alpha+\Phi_2\sin\alpha\ ,\\ \Phi_2'&=-\Phi_1\sin\alpha+\Phi_2\cos\alpha\ ,\end{aligned} \tag{3.3}$$

so that

$$\langle\Phi_1'\rangle=\frac{1}{\sqrt{2}}\begin{bmatrix}0\\ (a^2+b^2)^{1/2}\end{bmatrix},\quad \langle\Phi_2'\rangle=0 \tag{3.4}$$

and

$$\tan\alpha=\frac{b}{a}\ . \tag{3.5}$$

The field Φ_1' can be considered as the "true" Higgs field. To identify the physical fields we go to the unitary gauge and write

$$\begin{aligned}\Phi_1'\to U(\xi)\Phi_1'&=\begin{bmatrix}0\\ \frac{v+\eta}{\sqrt{2}}\end{bmatrix},\\ \Phi_2'\to U(\xi)\Phi_2'&=\begin{bmatrix}\chi\\ \frac{\phi+i\psi}{\sqrt{2}}\end{bmatrix},\end{aligned} \tag{3.6}$$

where $v^2=a^2+b^2$. The two scalar fields are ϕ and η, the pseudoscalar field is ψ, and the charged Higgs bosons are $\chi^{\pm}$. The general potential is given by[9]

$$\begin{aligned}V(\Phi_1,\Phi_2)=&-\mu_1{}^2\Phi_1^\dagger\Phi_1-\mu_2{}^2\Phi_2^\dagger\Phi_2+\lambda_1(\Phi_1^\dagger\Phi_1)^2\\ &+\lambda_2(\Phi_2^\dagger\Phi_2)^2+\lambda_3(\Phi_1^\dagger\Phi_1)(\Phi_2^\dagger\Phi_2)\\ &+\lambda_4|\Phi_1^\dagger\Phi_2|^2+\frac{\lambda_5}{2}[(\Phi_1^\dagger\Phi_2)^2+(\Phi_2^\dagger\Phi_1)^2]\ .\end{aligned} \tag{3.7}$$

The two scalars will in general mix and the mixing angle θ can be expressed in terms of the λ_i parameters in Eq. (3.7). The diagonalization of the η,ϕ fields is achieved through a rotation given by

$$\begin{aligned}\phi&=\tilde{\phi}\cos\theta+\tilde{\eta}\sin\theta\ ,\\ \eta&=-\tilde{\phi}\sin\theta+\tilde{\eta}\cos\theta\ .\end{aligned} \tag{3.8}$$

We shall treat θ as a parameter and now $\tilde{\phi}$ and $\tilde{\eta}$ are orthogonal. The masses of the spin-0 fields are

$$M_{\tilde{\phi},\tilde{\eta}}{}^2=\lambda_1 a^2+\lambda_2 b^2 \mp[(\lambda_1 a^2-\lambda_2 b^2)^2+a^2b^2\Lambda^2]^{1/2}, \quad M_\chi{}^2=-\tfrac{1}{2}(\lambda_4+\lambda_5)v^2, \quad M_\psi{}^2=-\lambda_5 v^2, \tag{3.9}$$

with $\Lambda=\lambda_3+\lambda_4+\lambda_5$. The parameters λ_4 and λ_5 can be chosen to be negative without loss of generality and hence (3.9) does not pose a consistency problem.

The interactions of Φ_1 and Φ_2 with the gauge bosons and fermions are given by $\mathcal{L}_g$ and $\mathcal{L}_y$, respectively. They are

$$\mathcal{L}_g=(D_\mu\Phi_1)^\dagger(D^\mu\Phi_1)+(D_\mu\Phi_2)^\dagger(D^\mu\Phi_2) \tag{3.10}$$

and

$$\mathcal{L}_y=y_1(\bar{u}_L\bar{d}_L)i\tau_2\Phi_1^* u_R+y_2(\bar{u}_L\bar{d}_L)\Phi_2 d_R +y_3(\bar{\nu}_L\bar{l}_L)\Phi_1 l_R+\text{H.c.} \tag{3.11}$$

One can rewrite the above in terms of the fields $\tilde{\eta}$, $\tilde{\phi}$, χ, and ψ using Eqs. (3.1)—(3.11), and obtain appropriate Feynman rules.

The vertices that will contribute to the two-photon decay width of the neutral spin-0 particle ($X=\tilde{\eta},\tilde{\phi},\psi$) are given in Table I. The magnitude and sign of the scalar coupling to charged Higgs bosons is highly model dependent and will be discussed below. As expected the pseudoscalar ψ is not affected by the mixing parameter θ. Also it does not couple to the W bosons or to the charged Higgs bosons. Hence, its production is the least model dependent. In general the scalar couplings to the W boson are smaller than in the standard model. For simplicity we take $\theta=0$. This in fact produces the constraint equation

$$\lambda_2 b^2-\lambda_1 a^2=\tfrac{1}{2}(b^2-a^2)(\lambda_3+\lambda_4+\lambda_5). \tag{3.12}$$

If all the λ_i's are of the same order, this equation can be naturally satisfied. With this choice of θ, the couplings for one of the scalars, $\tilde{\eta}$, become identical to those of the standard-model Higgs boson, and the other scalar does not couple to the W boson. Hence, we must look to the fermion loops for possible enhancement of the production rate.

There are two ways to enhance the contribution of the fermion loops. From Table I it can be seen that if $\tan\alpha$ ($\cot\alpha$) is large then the lepton and u-type quark loops will be enhanced (decreased), and the d-type quark loops decreased (enhanced). This is true for both the scalar and pseudoscalar bosons. In the standard six-quark world we found that only the t-quark loop made a significant contribution, and hence it is the logical one to try and enhance. Thus we will study the two-Higgs-doublet model with a large $\tan\alpha$ enhancement. The results for models with a large $\cot\alpha$ will be similar except that the cross sections one is enhancing are so much smaller to begin with.

The dominant contribution for both the scalar and pseudoscalar now comes from the t-quark loop enhanced by $\tan\alpha$. Bounds on the magnitude of the enhancement factor can be determined by low-energy phenomenology.[10] The virtual effects of the charged Higgs boson in e^+e^- collisions, muon decay, or the K_L^0-K_S^0 mass difference give $\tan\alpha$ an upper limit as a function of the charged-Higgs-boson mass M_χ. We use the approximate bound $\tan^2\alpha<2M_\chi/m_c$ from Ref. 11 where m_c is the charm-quark mass. Limits on M_χ can be obtained from considering their effects in the W- and Z-boson propagators. For $M_\chi \gg M_{\tilde{\eta}},M_{\tilde{\phi}}$ the change in the mass ratio of the gauge bosons is proportional to M_χ. Specifically $M_\chi=1.2$ TeV/c^2 will give a 5% change in the ρ parameter where $\rho\equiv M_W{}^2/M_Z{}^2\cos^2\theta_W$ (Ref. 12). This is within the experimental error allowed.[13] Taking all these together we get $\tan\alpha\lesssim 40$.

In the two-Higgs-doublet model there is an additional contribution to the 2γ decay width of the Higgs scalar coming from charged-Higgs-boson loops. The Feynman diagrams for this process are the same as those in Fig. 2(c), except the loop particle is a charged Higgs boson χ^+ rather than a would-be-Goldstone boson. The relevant scalar coupling to charged Higgs terms of the Lagrangian are

$$\chi^+\chi^-\tilde{\phi}\rightarrow v[-\lambda_1\sin^2\alpha+\lambda_2\cos^2\alpha-\tfrac{1}{2}\Lambda\cos(2\alpha)]\sin(2\alpha) \tag{3.13}$$

and

$$\chi^+\chi^-\tilde{\eta}\rightarrow v[\tfrac{1}{2}(\lambda_1+\lambda_2-\Lambda)\sin^2(2\alpha)+\lambda_3] \tag{3.14}$$

with $\theta=0$. The magnitude and sign of these couplings are not determined by the theory. But we have argued that $M_\chi\lesssim 1.2$ TeV/c^2 which means that λ_4 and λ_5 are of the

TABLE I. Yukawa and gauge couplings of scalars and pseudoscalar to fermions and W bosons for the two-Higgs-doublet model. The mixing angle of the two vacuum expectation values is α and the mixing angle between scalars is θ. The particle $X=H^0$, $\tilde{\eta}$, $\tilde{\phi}$, and ψ. The standard-model vertices for H^0 are shown for comparison.

Vertex	H^0	$\tilde{\eta}$	$\tilde{\phi}$	ψ
$e\bar{e}X$	$y_e=\dfrac{-im_e}{v}$	$y_e\dfrac{\cos(\theta+\alpha)}{\cos\alpha}$	$-y_e\dfrac{\sin(\theta+\alpha)}{\cos\alpha}$	$-y_e i\gamma_5\tan\alpha$
$u\bar{u}X$	$y_u=\dfrac{-im_u}{v}$	$y_u\dfrac{\cos(\theta+\alpha)}{\cos\alpha}$	$-y_u\dfrac{\sin(\theta+\alpha)}{\cos\alpha}$	$-y_u i\gamma_5\tan\alpha$
$d\bar{d}X$	$y_d=\dfrac{-im_d}{v}$	$y_d\dfrac{\sin(\theta+\alpha)}{\sin\alpha}$	$y_d\dfrac{\cos(\theta+\alpha)}{\sin\alpha}$	$y_d i\gamma_5\cot\alpha$
W^+W^-X	$g_W=\dfrac{ig^2v}{2}g_{\mu\nu}$	$g_W\cos\theta$	$-g_W\sin\theta$	0

order of unity. It is natural to assume that all the λ's are of the same order. This argument is by no means rigorous but is supported by partial-wave unitarity plus perturbation theory,[14] which gives a similar bound on M_χ. With these caveats we see from Eqs. (3.13) and (3.14) that $\chi^+\chi^-\tilde{\phi}$ and $\chi^+\chi^-\tilde{\eta}$ are not enhanced. Hence the χ loops are not big contributors to A.

Now we calculate the production cross sections for the processes in Eq. (1.1) with the EPA for the two-Higgs-doublet model. For the scalar particles the results from the standard model still hold, with the exception that now the amplitude A in Eq. (2.2) contains fermion-loop contributions multiplied by the appropriate enhancement factors from Table I. For the pseudoscalar we calculate the cross section for subprocess Eq. (1.2b) using the EPA and obtain

$$\hat{\sigma}_q(\hat{s})=\frac{\alpha^2 Q_q{}^2|A|^2}{4\pi M_H{}^4}\ln\left[\frac{\hat{s}}{m_e{}^2}\right]\left[\ln\left[\frac{M_H{}^2}{m_q{}^2}\right][\rho^2+2\rho-3-(2+2\rho+\tfrac{1}{2}\rho^2)\ln\rho]\right.$$
$$+\tfrac{1}{2}(2+2\rho+\tfrac{1}{2}\rho^2)\ln^2\rho-2(3-2\rho-\rho^2)\ln(1-\rho)+(6-4\rho-\tfrac{7}{4}\rho^2)\ln\rho$$
$$\left.+\tfrac{1}{8}(47-28\rho-19\rho^2)+2(2+2\rho+\tfrac{1}{2}\rho^2)[-\mathrm{Li}(1)+\mathrm{Li}(\rho)+\tfrac{1}{2}\ln^2\rho]\right], \tag{3.15}$$

where ρ, $\hat{s}$, and $\mathrm{Li}(x)$ are as defined in Eq. (2.3). Here

$$A=\frac{-ie^2gM_H{}^2}{8\pi^2M_W}\sum_f\frac{Q_f{}^2m_f{}^2}{M_H{}^2}I\left[\frac{m_f{}^2}{M_H{}^2}\right]E_f \tag{3.16}$$

with $I(\lambda)$ as defined in Eq. (2.2e), and the appropriate enhancement factors E_f are from Table I. Again we convolute over quark distributions with Eq. (2.4) to obtain the production cross sections for the processes of Eq. (1.1). The specific quark distributions we used are given in Ref. 15.

Plots of the enhanced cross sections as a function of Higgs-boson mass, using $\tan\alpha=40$, are compared to the standard model in Figs. 4 and 5 for $\sqrt{s}=320$ GeV and 1 TeV, respectively. Again we notice a peak in the cross sections of Fig. 5 due to the behavior of $I(\lambda=M_t{}^2/M_W{}^2)$). However in this case the t-quark loop dominates so $\lambda=\frac{1}{4}$ corresponds to $M_H=2m_t$. As expected the pseudoscalar cross-section equation (3.16) peaks just past $M_H=80$ GeV/c^2. In the scalar case the peak is less pronounced and is situated at larger M_H due to the factor $(4\lambda-1)$ which multiplies $I(\lambda)$ in Eq. (2.2c). Hence the peak due to $\mathrm{Re}[I(\lambda)]$ at $\lambda=\frac{1}{4}$ is suppressed and it is the imaginary part of $I(\lambda)$ at $\lambda>\frac{1}{4}$ which gives rise to the peak. Similar behavior in Fig. 4 is somewhat obscured since the more restrictive phase space dominates the shape of the cross section. For a range of Higgs-boson masses, the enhanced photon-exchange cross sections are much larger than the Z^0-boson fusion mechanism by roughly an order of magnitude. The pseudoscalar rate is about three times that of the scalar. Although the actual cross sections for a two-Higgs-doublet model may fall below the bounds shown, reasonably large cross sections (up to 10^{-37} cm^2) are possible even at HERA energies. Folding in the luminosity gives a rate of 180 events per year of running. Hence one may be able to observe Higgs-boson production in ep collisions within the context of the two-Higgs-doublet model. Furthermore the rates can again be enhanced with the addition of heavy u-type quarks. Unlike the standard model, large numbers of families are not needed since there is no gauge-boson loop to cancel. Even the addition of only one extra heavy fermion can roughly quadruple the rate.

Plots of the enhanced ($\tan\alpha=40$) photon-exchange cross sections for $e^+e^-\to e^+e^-H^0$ are given in Fig. 6. The variation of cross section with $\sqrt{s}$ for $M_H=60$ GeV/c^2, and the cross section versus M_H for $\sqrt{s}=150$ GeV are displayed. These values were chosen to facilitate

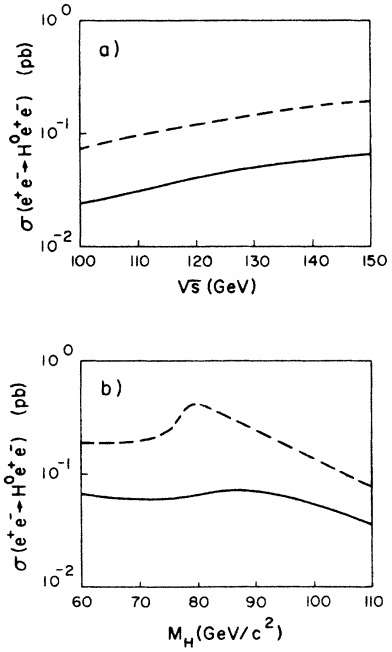

FIG. 6. Production cross sections for $e\bar{e}\to e\bar{e}H^0$ as a function of (a) $\sqrt{s}$ for $M_H=60$ GeV/c^2, (b) M_H for $\sqrt{s}=150$ GeV. The solid (broken) curve is for two-Higgs-doublet model photon-exchange scalar (pseudoscalar) production with $\tan\alpha=40$.

comparison with the standard-model graphs given in Ref. 5. The behavior is similar to that found for *ep* scattering above. The peak in the total cross section versus M_H distribution is sharper since there is no smearing by the parton distributions. The enhanced cross section is roughly an order of magnitude larger than the standard-model process one (see Ref. 5).

IV. DISCUSSION

Using the two-doublets extension of the standard SU(2)×U(1) electroweak model, we have calculated the production cross sections for a scalar ($\tilde{\eta},\tilde{\phi}$) or pseudoscalar ($\psi$) in *ep* and e^+e^- collisions for a mass range of 40 to 150 GeV/c^2. This is the mass range accessible to HERA and LEP.

The largest uncertainty of the calculation lies in the charged-Higgs-boson loops [see Fig. 2(c)] but fortunately their contribution is negligible if the parameters in the scalar potential are not large. If not we encounter either strongly interacting scalars or vacuum instability. Thus using only phenomenological constraints[16] on the mixing of the two VEV's we found that larger production rates than in the standard model are possible by enhancing the fermion loops [see Fig. 2(a)]. In the best case the *t*-quark loop is enhanced by the largest value of $\tan\alpha=40$. This occurs for both the pseudoscalar and *one* of the scalar Higgs bosons. The other scalar would behave as in the standard model but with the gauge-boson loop suppressed, and its production rate would then be too small to be of interest.

As in the standard model, the scalar or pseudoscalar bosons will decay primarily into a pair of heavy quarks. Thus our signal will be two jets from the Higgs-boson decay. In Fig. 7 the rapidity distributions of the Higgs-boson scalar for *ep* and $e\bar{e}$ photon-exchange mechanisms are given. The pseudoscalar rapidity distributions are similar. In both cases the rapidity is broadly peaked about the center. For the $e\bar{e}\to e\bar{e}H^0$ process, the laboratory frame and the c.m. frame coincide. The two Higgs-boson decay jets should therefore stand out well away from the beam axis, providing a good signal. However in the $ep\to eH^0X$ process, the c.m. frame has a large velocity in the laboratory frame. The resulting boost will shift the scale on the rapidity distribution in Fig. 7(a) by roughly -1.6 at HERA. Hence in the laboratory frame the rapidity distribution will peak at less than 10° from the beam axis, and at least one of the decay jets may be difficult to distinguish from the beam jets. In order to resolve this problem, much higher event rates may be needed for *ep* colliders than for $e\bar{e}$ machines.

The *ep* event rates discussed below are for HERA assuming $\sqrt{s}=320$ GeV and an integrated luminosity over one year's running of 1.89×10^{39} cm^{-2}. The $e\bar{e}$ rates are for SLC assuming $\sqrt{s}=100$ GeV and an integrated luminosity of 9.45×10^{37} cm^{-2}. In the standard model, Higgs-boson production is dominated by the *Z*-boson-exchange mechanism and the event rates of <3 per year

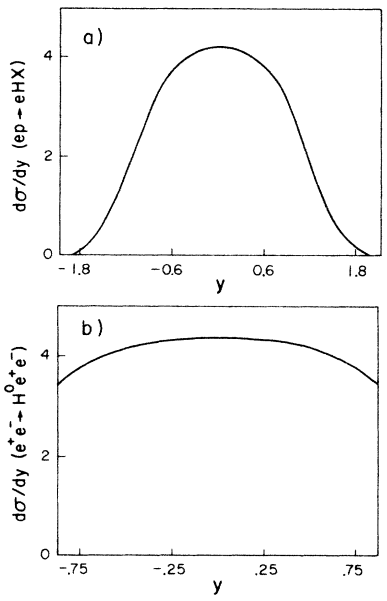

FIG. 7. Scalar-boson rapidity distribution in the c.m. frame for (a) $ep\to eH^0X$ with $\sqrt{s}=320$ GeV and $M_H=40$ GeV/c^2, (b) $e\bar{e}\to e\bar{e}H^0$ with $\sqrt{s}=150$ GeV and $M_H=60$ GeV/c^2. The normalization is arbitrary.

are too small to be observed. Only the inclusion of incredibly large numbers of heavy fermions in the photon-exchange process can bring the rates up to observable levels. On the other hand, the cross sections for the two-Higgs-doublet model can be quite substantial. This is due to the possibility of enhancing the Yukawa coupling of the *t* quark in this model. We also demonstrated the charged scalars do not give large contributions to the effective $P^0\gamma\gamma$ or $S^0\gamma\gamma$ couplings. We calculate upper bound estimates on the event rates in *ep* colliders of $\lesssim65$ for the scalar boson and $\lesssim176$ for the pseudoscalar without folding in the detection efficiency. In $e\bar{e}$ collisions the corresponding event rates are $\lesssim2$ for the scalar and $\lesssim13$ for the pseudoscalar. These rates can be further enhanced if there are additional heavy fermions in the model.

Although the cleaner signal may be found with $e\bar{e}$ machines, our upper bound production rates are not very large. A higher-luminosity $e\bar{e}$ machine, perhaps the proposed LEP II at CERN, would be useful in providing both larger rates and a clean signal. On the other hand, the *ep* production rates are much larger, especially for the pseudoscalar boson. Hence we conclude that it may be possible to detect nonstandard Higgs bosons in *ep* colliders such as HERA.

ACKNOWLEDGMENT

One of the authors (J.N.N.) would like to thank the Aspen Institute of Physics for its kind hospitality. Part of this work was done while he was visiting there.

[1]R. J. Cashmore, in *Proceedings of the Study of an ep Facility for Europe,* edited by U. Amaldi (DESY, Hamburg, 1979).
[2]H. E. Haber and G. L. Kane, Phys. Rep. **117**, 76 (1985).
[3]K. F. Weizsacker, Z. Phys. **88**, 612 (1934); E. J. Williams, Phys. Rev. **45**, 729 (1934).
[4]D. R. T. Jones and S. T. Petcov, Phys. Lett. **84B**, 440 (1979).
[5]R. Bates and J. N. Ng, Phys. Rev. D **32**, 51 (1985).
[6]A. Dicus and D. Willenbrock, University of Texas report, 1985 (unpublished).
[7]J. Ellis, M. K. Gaillard, and D. V. Nanopoulos, Nucl. Phys. **B106**, 292 (1976).
[8]A. N. Kamal, J. N. Ng, and H. C. Lee, Phys. Rev. D **24**, 2842 (1981).
[9]R. A. Flores and M. Sher, Ann. Phys. (N.Y.) **148**, 95 (1981).
[10]H. E. Haber, G. L. Kane, and T. Sterling, Nucl. Phys. **B161**, 493 (1979); J. N. Ng, Phys. Rev. D **31**, 464 (1985); Y. P. Nikitin, D. V. Pikhterev, and S. G. Rubin, Yad. Fiz. **36**, 180 (1982) [Sov. J. Nucl. Phys. **36**, 106 (1982)].
[11]L. F. Abbott, P. Sikivie, and M. B. Wise, Phys. Rev. D **21**, 1393 (1980).
[12]D. Toussiant, Phys. Rev. D **18**, 1626 (1978).
[13]UA1 Collaboration, G. Arnison *et al.*, Phys. Lett. **122B**, 103 (1983); **126B**, 398 (1983); UA2 Collaboration, M. Banner *et al.*, *ibid.* **122B**, 476 (1983); **129B**, 130 (1983).
[14]B. W. Lee, C. Quigg, and H. B. Thacker, Phys. Rev. D **16**, 1519 (1977); H. Huffel and G. Pocsik, Z. Phys. C **8**, 13 (1981).
[15]R. Baier, J. Engels, and B. Petersson, Z. Phys. C **6**, 309 (1980).
[16]We have not used perturbative partial-wave unitarity constraints. See M. S. Chanowitz, M. A. Furman, and I. Hinchliffe, Nucl. Phys. **B153**, 402 (1979). This will lead to $\tan\alpha \lesssim 12$ for enhancing t quarks. If one adopts this then our numerical results should be scaled accordingly.